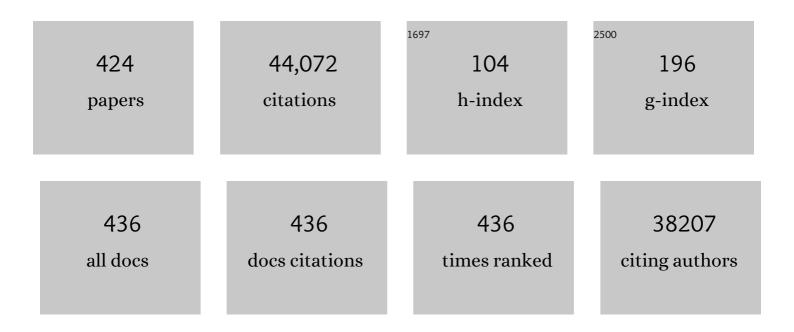
List of Publications by Year in descending order

Source: https://exaly.com/author-pdf/3315779/publications.pdf Version: 2024-02-01



#	Article	IF	CITATIONS
1	Localized $\hat{a} {\in} \mathbf{d}$ omains staging structure and evolution in lithiated graphite. , 2023, 5, .		21
2	Moiré Fringe Method via Scanning Transmission Electron Microscopy. Small Methods, 2022, 6, e2101040.	4.6	25
3	Understanding the structural dynamics of electrocatalysts via liquid cell transmission electron microscopy. Current Opinion in Electrochemistry, 2022, 33, 100936.	2.5	7
4	Ensemble Machineâ€Learningâ€Based Analysis for In Situ Electron Diffraction. Advanced Theory and Simulations, 2022, 5, .	1.3	7
5	Topologically protected oxygen redox in a layered manganese oxide cathode for sustainable batteries. Nature Sustainability, 2022, 5, 214-224.	11.5	44
6	Passive Oxide Film Growth Observed On the Atomic Scale. Advanced Materials Interfaces, 2022, 9, .	1.9	4
7	Enhancing CO Oxidation Activity <i>via</i> Tuning a Charge Transfer Between Gold Nanoparticles and Supports. Journal of Physical Chemistry C, 2022, 126, 4836-4844.	1.5	1
8	Structure modification of Ni-rich layered oxide cathode toward advanced lithium-ion batteries. Journal of Materials Research, 2022, 37, 3250-3268.	1.2	4
9	A self-purifying electrolyte enables high energy Li ion batteries. Energy and Environmental Science, 2022, 15, 3331-3342.	15.6	40
10	Quasi-Covalently Coupled Ni–Cu Atomic Pair for Synergistic Electroreduction of CO ₂ . Journal of the American Chemical Society, 2022, 144, 9661-9671.	6.6	134
11	Rhombohedral Pd–Sb Nanoplates with Pdâ€Terminated Surface: An Efficient Bifunctional Fuelâ€Cell Catalyst. Advanced Materials, 2022, 34, .	11.1	33
12	A laminated carbon nanotubes/silicon boron carbonitride film for high-efficiency electromagnetic interference shielding with oxidation resistance. Carbon, 2022, 197, 65-75.	5.4	11
13	Engineering Atomically Dispersed FeN ₄ Active Sites for CO ₂ Electroreduction. Angewandte Chemie, 2021, 133, 1035-1045.	1.6	39
14	In Operando Visualization of Cation Disorder Unravels Voltage Decay in Niâ€Rich Cathodes. Small Methods, 2021, 5, e2000730.	4.6	18
15	Engineering Atomically Dispersed FeN ₄ Active Sites for CO ₂ Electroreduction. Angewandte Chemie - International Edition, 2021, 60, 1022-1032.	7.2	121
16	On the irreversible sodiation of tin disulfide. Nano Energy, 2021, 79, 105458.	8.2	14
17	WO <i>_x</i> â€Surface Decorated PtNi@Pt Dendritic Nanowires as Efficient pHâ€Universal Hydrogen Evolution Electrocatalysts. Advanced Energy Materials, 2021, 11, 2003192.	10.2	82
18	Cationic–anionic redox couple gradient to immunize against irreversible processes of Li-rich layered oxides. Journal of Materials Chemistry A, 2021, 9, 2325-2333.	5.2	20

#	Article	IF	CITATIONS
19	High-temperature-pulse synthesis of ultrathin-graphene-coated metal nanoparticles. Nano Energy, 2021, 80, 105536.	8.2	9
20	Effect of SiO2 deposition on thermal stability of Al2O3-SiO2 aerogel. Journal of the European Ceramic Society, 2021, 41, 580-589.	2.8	33
21	Dual-stage K ⁺ ion intercalation in V ₂ O ₅ -conductive polymer composites. Journal of Materials Chemistry A, 2021, 9, 15629-15636.	5.2	13
22	Non-equilibrium insertion of lithium ions into graphite. Journal of Materials Chemistry A, 2021, 9, 12080-12086.	5.2	15
23	A highly efficient atomically thin curved PdIr bimetallene electrocatalyst. National Science Review, 2021, 8, nwab019.	4.6	59
24	Real Time Observation of Lithium Insertion into Pre-Cycled Conversion-Type Materials. Nanomaterials, 2021, 11, 728.	1.9	3
25	Dynamically Unveiling Metal–Nitrogen Coordination during Thermal Activation to Design Highâ€Efficient Atomically Dispersed CoN ₄ Active Sites. Angewandte Chemie - International Edition, 2021, 60, 9516-9526.	7.2	119
26	Dynamically Unveiling Metal–Nitrogen Coordination during Thermal Activation to Design Highâ€Efficient Atomically Dispersed CoN ₄ Active Sites. Angewandte Chemie, 2021, 133, 9602-9612.	1.6	21
27	Near-room temperature ferromagnetic insulating state in highly distorted LaCoO2.5 with CoO5 square pyramids. Nature Communications, 2021, 12, 1853.	5.8	25
28	Shielded SnS2/SnS heterostructures on three-dimensional graphene framework for high-rate and stable sodium-ion storage. Electrochimica Acta, 2021, 372, 137800.	2.6	27
29	Layered-rocksalt intergrown cathode for high-capacity zero-strain battery operation. Nature Communications, 2021, 12, 2348.	5.8	43
30	Deciphering Interfacial Chemical and Electrochemical Reactions of Sulfideâ€Based Allâ€Solidâ€State Batteries. Advanced Energy Materials, 2021, 11, 2100210.	10.2	63
31	Structural Changes of Intermetallic Catalysts under Reaction Conditions. Small Structures, 2021, 2, 2100011.	6.9	21
32	3d-Orbital Occupancy Regulated Ir-Co Atomic Pair Toward Superior Bifunctional Oxygen Electrocatalysis. ACS Catalysis, 2021, 11, 8837-8846.	5.5	110
33	Thermal radiation shielded, high strength, fire resistant fiber/nanorod/aerogel composites fabricated by in-situ growth of TiO2 nanorods for thermal insulation. Chemical Engineering Journal, 2021, 418, 129342.	6.6	44
34	High-performance ammonia oxidation catalysts for anion-exchange membrane direct ammonia fuel cells. Energy and Environmental Science, 2021, 14, 1449-1460.	15.6	100
35	Atomic Structure Evolution of Pt–Co Binary Catalysts: Single Metal Sites versus Intermetallic Nanocrystals. Advanced Materials, 2021, 33, e2106371.	11.1	62
36	Dynamics of Anisotropic Oxygen-Ion Migration in Strained Cobaltites. Nano Letters, 2021, 21, 10507-10515.	4.5	9

#	Article	IF	CITATIONS
37	A graphene-modified flexible SiOC ceramic cloth for high-performance lithium storage. Energy Storage Materials, 2020, 25, 876-884.	9.5	53
38	NbOx nano-nail with a Pt head embedded in carbon as a highly active and durable oxygen reduction catalyst. Nano Energy, 2020, 69, 104455.	8.2	37
39	Molecular-Level Proximity of Metal and Acid Sites in Zeolite-Encapsulated Pt Nanoparticles for Selective Multistep Tandem Catalysis. ACS Catalysis, 2020, 10, 3340-3348.	5.5	50
40	A multifunctional hierarchical porous SiO2/GO membrane for high efficiency oil/water separation and dye removal. Carbon, 2020, 160, 88-97.	5.4	117
41	Boosting CO2 reduction on Fe-N-C with sulfur incorporation: Synergistic electronic and structural engineering. Nano Energy, 2020, 68, 104384.	8.2	106
42	Site-Specific Sodiation Mechanisms of Selenium in Microporous Carbon Host. Nano Letters, 2020, 20, 918-928.	4.5	30
43	A Triphasic Bifunctional Oxygen Electrocatalyst with Tunable and Synergetic Interfacial Structure for Rechargeable Znâ€Air Batteries. Advanced Energy Materials, 2020, 10, 1903003.	10.2	74
44	Bi-continuous nanoporous carbon sphere derived from SiOC as high-performance anodes for PIBs. Chemical Engineering Journal, 2020, 381, 122677.	6.6	46
45	In Situ Transmission Electron Microscopy on Energyâ€Related Catalysis. Advanced Energy Materials, 2020, 10, 1902105.	10.2	78
46	Single Cobalt Sites Dispersed in Hierarchically Porous Nanofiber Networks for Durable and Highâ€Power PGMâ€Free Cathodes in Fuel Cells. Advanced Materials, 2020, 32, e2003577.	11.1	262
47	Direct Observation of Defectâ€Aided Structural Evolution in a Nickelâ€Rich Layered Cathode. Angewandte Chemie, 2020, 132, 22276-22283.	1.6	15
48	Direct Observation of Defectâ€Aided Structural Evolution in a Nickelâ€Rich Layered Cathode. Angewandte Chemie - International Edition, 2020, 59, 22092-22099.	7.2	75
49	Single-Iron Site Catalysts with Self-Assembled Dual-size Architecture and Hierarchical Porosity for Proton-Exchange Membrane Fuel Cells. Applied Catalysis B: Environmental, 2020, 279, 119400.	10.8	94
50	High thermal stability of SiO2–ZrO2 aerogels using solvent-thermal aging. Journal of Solid State Chemistry, 2020, 291, 121624.	1.4	19
51	Tensile-strained ruthenium phosphide by anion substitution for highly active and durable hydrogen evolution. Nano Energy, 2020, 77, 105212.	8.2	39
52	Undercoordinated Active Sites on 4H Gold Nanostructures for CO ₂ Reduction. Nano Letters, 2020, 20, 8074-8080.	4.5	46
53	Multimodal Analysis of Reaction Pathways of Cathode Materials for Lithium Ion Batteries. Microscopy and Microanalysis, 2020, 26, 906-908.	0.2	0
54	Atomically Dispersed MnN ₄ Catalysts <i>via</i> Environmentally Benign Aqueous Synthesis for Oxygen Reduction: Mechanistic Understanding of Activity and Stability Improvements. ACS Catalysis, 2020, 10, 10523-10534.	5.5	123

#	Article	IF	CITATIONS
55	Tuning the Anode–Electrolyte Interface Chemistry for Garnetâ€Based Solid‣tate Li Metal Batteries. Advanced Materials, 2020, 32, e2000030.	11.1	156
56	A Flexible Film with SnS ₂ Nanoparticles Chemically Anchored on 3Dâ€Graphene Framework for High Areal Density and High Rate Sodium Storage. Small, 2020, 16, e2001265.	5.2	23
57	A Highly Efficient Allâ€Solidâ€State Lithium/Electrolyte Interface Induced by an Energetic Reaction. Angewandte Chemie - International Edition, 2020, 59, 14003-14008.	7.2	70
58	A Highly Efficient Allâ€Solidâ€State Lithium/Electrolyte Interface Induced by an Energetic Reaction. Angewandte Chemie, 2020, 132, 14107-14112.	1.6	4
59	Hierarchical Polyelemental Nanoparticles as Bifunctional Catalysts for Oxygen Evolution and Reduction Reactions. Advanced Energy Materials, 2020, 10, 2001119.	10.2	39
60	Single crystal cathodes enabling high-performance all-solid-state lithium-ion batteries. Energy Storage Materials, 2020, 30, 98-103.	9.5	109
61	Imaging the kinetics of anisotropic dissolution of bimetallic core–shell nanocubes using graphene liquid cells. Nature Communications, 2020, 11, 3041.	5.8	36
62	Harnessing strong metal–support interactions via a reverse route. Nature Communications, 2020, 11, 3042.	5.8	84
63	Surface regulation enables high stability of single-crystal lithium-ion cathodes at high voltage. Nature Communications, 2020, 11, 3050.	5.8	225
64	Tuning epitaxial growth on NaYbF ₄ upconversion nanoparticles by strain management. Nanoscale, 2020, 12, 13973-13979.	2.8	14
65	Biaxial Strains Mediated Oxygen Reduction Electrocatalysis on Fenton Reaction Resistant L1 ₀ â€PtZn Fuel Cell Cathode. Advanced Energy Materials, 2020, 10, 2000179.	10.2	112
66	Deep learning analysis on microscopic imaging in materials science. Materials Today Nano, 2020, 11, 100087.	2.3	82
67	Lead-Free Cs ₄ CuSb ₂ Cl ₁₂ Layered Double Perovskite Nanocrystals. Journal of the American Chemical Society, 2020, 142, 11927-11936.	6.6	131
68	Unveiling the critical role of interfacial ionic conductivity in all-solid-state lithium batteries. Nano Energy, 2020, 72, 104686.	8.2	56
69	C–O bond activation using ultralow loading of noble metal catalysts on moderately reducible oxides. Nature Catalysis, 2020, 3, 446-453.	16.1	131
70	Supported and coordinated single metal site electrocatalysts. Materials Today, 2020, 37, 93-111.	8.3	71
71	Ternary PtIrNi Catalysts for Efficient Electrochemical Ammonia Oxidation. ACS Catalysis, 2020, 10, 3945-3957.	5.5	104
72	Revealing Reaction Pathways of Collective Substituted Iron Fluoride Electrode for Lithium Ion Batteries. ACS Nano, 2020, 14, 10276-10283.	7.3	14

#	Article	IF	CITATIONS
73	Highly dispersed Co deposited on Al ₂ O ₃ particles via CoCp ₂ + H ₂ ALD. Nanotechnology, 2020, 31, 175703.	1.3	4
74	Interatomic diffusion in Pd-Pt core-shell nanoparticles. Chinese Journal of Catalysis, 2020, 41, 807-812.	6.9	4
75	Programmable Synthesis of Multimetallic Phosphide Nanorods Mediated by Core/Shell Structure Formation and Conversion. Journal of the American Chemical Society, 2020, 142, 8490-8497.	6.6	65
76	Overcoming immiscibility toward bimetallic catalyst library. Science Advances, 2020, 6, eaaz6844.	4.7	105
77	Electrolyte design for LiF-rich solid–electrolyte interfaces to enable high-performance microsized alloy anodes for batteries. Nature Energy, 2020, 5, 386-397.	19.8	621
78	A "trimurti" heterostructured hybrid with an intimate CoO/Co _x P interface as a robust bifunctional air electrode for rechargeable Zn–air batteries. Journal of Materials Chemistry A, 2020, 8, 9177-9184.	5.2	72
79	In-situ TEM Investigation of Lithiation and Sodiation of 2D Metal Sulfides. Microscopy and Microanalysis, 2020, 26, 1098-1100.	0.2	0
80	Ultrathin two-dimensional metallic nanocrystals for renewable energy electrocatalysis. Materials Today, 2019, 23, 45-56.	8.3	64
81	<i>In Situ</i> Electron Microscopy Investigation of Sodiation of Titanium Disulfide Nanoflakes. ACS Nano, 2019, 13, 9421-9430.	7.3	30
82	Enhancing C–C Bond Scission for Efficient Ethanol Oxidation using PtIr Nanocube Electrocatalysts. ACS Catalysis, 2019, 9, 7618-7625.	5.5	79
83	3D porous graphitic nanocarbon for enhancing the performance and durability of Pt catalysts: a balance between graphitization and hierarchical porosity. Energy and Environmental Science, 2019, 12, 2830-2841.	15.6	219
84	Expanded lithiation of titanium disulfide: Reaction kinetics of multi-step conversion reaction. Nano Energy, 2019, 63, 103882.	8.2	21
85	Exploring Metal–Support Interactions To Immobilize Subnanometer Co Clusters on γ–Mo ₂ N: A Highly Selective and Stable Catalyst for CO ₂ Activation. ACS Catalysis, 2019, 9, 9087-9097.	5.5	50
86	Tungstenâ€Doped L1 0 â€₽tCo Ultrasmall Nanoparticles as a Highâ€Performance Fuel Cell Cathode. Angewandte Chemie, 2019, 131, 15617-15623.	1.6	30
87	High-performance layered NiCo2S4@rGO/rGO film electrode for flexible electrochemical energy storage. Electrochimica Acta, 2019, 328, 135088.	2.6	33
88	PdAu Alloy Nanoparticles for Ethanol Oxidation in Alkaline Conditions: Enhanced Activity and C1 Pathway Selectivity. ACS Applied Energy Materials, 2019, 2, 8701-8706.	2.5	45
89	Highly Efficient AuPd Catalyst for Synthesizing Polybenzoxazole with Controlled Polymerization. Matter, 2019, 1, 1631-1643.	5.0	8
90	Framework Doping of Ni Enhances Pseudocapacitive Na-Ion Storage of (Ni)MnO ₂ Layered Birnessite. Chemistry of Materials, 2019, 31, 8774-8786.	3.2	51

#	Article	IF	CITATIONS
91	Single Atom Identification of Barium by HAADF-STEM for the New Enriched Xenon Observatory (nEXO). Microscopy and Microanalysis, 2019, 25, 670-671.	0.2	0
92	Highly Dispersed Platinum Atoms on the Surface of AuCu Metallic Aerogels for Enabling H ₂ O ₂ Production. ACS Applied Energy Materials, 2019, 2, 7722-7727.	2.5	31
93	Cu ₃ N Nanocubes for Selective Electrochemical Reduction of CO ₂ to Ethylene. Nano Letters, 2019, 19, 8658-8663.	4.5	173
94	Unraveling the Voltage Decay Phenomenon in Liâ€Rich Layered Oxide Cathode of No Oxygen Activity. Advanced Energy Materials, 2019, 9, 1902258.	10.2	51
95	Quinary Defect-Rich Ultrathin Bimetal Hydroxide Nanosheets for Water Oxidation. ACS Applied Materials & Interfaces, 2019, 11, 44018-44025.	4.0	15
96	Tungstenâ€Doped L1 ₀ â€PtCo Ultrasmall Nanoparticles as a Highâ€Performance Fuel Cell Cathode. Angewandte Chemie - International Edition, 2019, 58, 15471-15477.	7.2	150
97	Accurate Control of Core–Shell Upconversion Nanoparticles through Anisotropic Strain Engineering. Advanced Functional Materials, 2019, 29, 1903295.	7.8	59
98	In-situ TEM Investigation on Reaction Mechanisms of Conversion Electrode Materials for Batteries. Microscopy and Microanalysis, 2019, 25, 1434-1435.	0.2	0
99	General Synthetic Route to High-Quality Colloidal III–V Semiconductor Quantum Dots Based on Pnictogen Chlorides. Journal of the American Chemical Society, 2019, 141, 15145-15152.	6.6	54
100	Trifunctional Fishbone-like PtCo/Ir Enables High-Performance Zinc–Air Batteries to Drive the Water-Splitting Catalysis. Chemistry of Materials, 2019, 31, 8136-8144.	3.2	55
101	Ensemble Effect in Bimetallic Electrocatalysts for CO ₂ Reduction. Journal of the American Chemical Society, 2019, 141, 16635-16642.	6.6	238
102	Generalized Synthetic Strategy for Transition-Metal-Doped Brookite-Phase TiO ₂ Nanorods. Journal of the American Chemical Society, 2019, 141, 16548-16552.	6.6	78
103	PdMo bimetallene for oxygen reduction catalysis. Nature, 2019, 574, 81-85.	13.7	935
104	Tailoring FeN ₄ Sites with Edge Enrichment for Boosted Oxygen Reduction Performance in Proton Exchange Membrane Fuel Cell. Advanced Energy Materials, 2019, 9, 1803737.	10.2	148
105	Highly active atomically dispersed CoN ₄ fuel cell cathode catalysts derived from surfactant-assisted MOFs: carbon-shell confinement strategy. Energy and Environmental Science, 2019, 12, 250-260.	15.6	691
106	A Singleâ€Atom Iridium Heterogeneous Catalyst in Oxygen Reduction Reaction. Angewandte Chemie, 2019, 131, 9742-9747.	1.6	59
107	Rücktitelbild: A Singleâ€Atom Iridium Heterogeneous Catalyst in Oxygen Reduction Reaction (Angew.) Tj ETQo	1 1 0.78 1 1.6	1314 rgBT /0 1
108	Development of a water cycle management approach to Sponge City construction in Xi'an, China. Science of the Total Environment, 2019, 685, 490-496.	3.9	26

#	Article	IF	CITATIONS
109	SO ₂ -Induced Selectivity Change in CO ₂ Electroreduction. Journal of the American Chemical Society, 2019, 141, 9902-9909.	6.6	102
110	A Singleâ€Atom Iridium Heterogeneous Catalyst in Oxygen Reduction Reaction. Angewandte Chemie - International Edition, 2019, 58, 9640-9645.	7.2	312
111	Modulating the electronic structure of ultrathin layered double hydroxide nanosheets with fluorine: an efficient electrocatalyst for the oxygen evolution reaction. Journal of Materials Chemistry A, 2019, 7, 14483-14488.	5.2	73
112	Tuning CO2 hydrogenation selectivity via metal-oxide interfacial sites. Journal of Catalysis, 2019, 374, 60-71.	3.1	115
113	Phase evolution of conversion-type electrode for lithium ion batteries. Nature Communications, 2019, 10, 2224.	5.8	99
114	Large-diameter and heteroatom-doped graphene nanotubes decorated with transition metals as carbon hosts for lithium–sulfur batteries. Journal of Materials Chemistry A, 2019, 7, 13389-13399.	5.2	27
115	Atomic Arrangement Engineering of Metallic Nanocrystals for Energy-Conversion Electrocatalysis. Joule, 2019, 3, 956-991.	11.7	197
116	Quantification of Charge Transfer at the Interfaces of Oxide Thin Films. Journal of Physical Chemistry A, 2019, 123, 4632-4637.	1.1	5
117	Cu-Catalyzed Synthesis of CdZnSe–CdZnS Alloy Quantum Dots with Highly Tunable Emission. Chemistry of Materials, 2019, 31, 2635-2643.	3.2	41
118	Fuel Cells: Tailoring FeN ₄ Sites with Edge Enrichment for Boosted Oxygen Reduction Performance in Proton Exchange Membrane Fuel Cell (Adv. Energy Mater. 11/2019). Advanced Energy Materials, 2019, 9, 1970031.	10.2	7
119	Highly Active Ceria-Supported Ru Catalyst for the Dry Reforming of Methane: In Situ Identification of Ru ^{Î+} –Ce ³⁺ Interactions for Enhanced Conversion. ACS Catalysis, 2019, 9, 3349-3359.	5.5	135
120	Tuning infrared plasmon resonances in doped metal-oxide nanocrystals through cation-exchange reactions. Nature Communications, 2019, 10, 1394.	5.8	64
121	Atomically Dispersed Iron Cathode Catalysts Derived from Binary Ligand-Based Zeolitic Imidazolate Frameworks with Enhanced Stability for PEM Fuel Cells. Journal of the Electrochemical Society, 2019, 166, F3116-F3122.	1.3	31
122	Zinc–Air Batteries: An Oxygenâ€Vacancyâ€Rich Semiconductorâ€Supported Bifunctional Catalyst for Efficient and Stable Zinc–Air Batteries (Adv. Mater. 6/2019). Advanced Materials, 2019, 31, 1970043.	11.1	3
123	Ultrathin PtNiM (M = Rh, Os, and Ir) Nanowires as Efficient Fuel Oxidation Electrocatalytic Materials. Advanced Materials, 2019, 31, e1805833.	11.1	223
124	Inâ€situ structural characterizations of electrochemical intercalation of graphite compounds. , 2019, 1, 200-218.		50
125	Defectsâ€Induced Inâ€Plane Heterophase in Cobalt Oxide Nanosheets for Oxygen Evolution Reaction. Small, 2019, 15, e1904903.	5.2	69
126	Chemical Synthesis of Magnetically Hard and Strong Rare Earth Metal Based Nanomagnets. Angewandte Chemie - International Edition, 2019, 58, 602-606.	7.2	42

#	Article	IF	CITATIONS
127	Chemical Synthesis of Magnetically Hard and Strong Rare Earth Metal Based Nanomagnets. Angewandte Chemie, 2019, 131, 612-616.	1.6	9
128	In Situ Transmission Electron Microscopy for Energy Applications. Joule, 2019, 3, 4-8.	11.7	69
129	Electrolyte Concentration Effect on Sulfur Utilization of Li-S Batteries. Journal of the Electrochemical Society, 2019, 166, A50-A58.	1.3	18
130	Size-dependent kinetics during non-equilibrium lithiation of nano-sized zinc ferrite. Nature Communications, 2019, 10, 93.	5.8	39
131	Mn- and N- doped carbon as promising catalysts for oxygen reduction reaction: Theoretical prediction and experimental validation. Applied Catalysis B: Environmental, 2019, 243, 195-203.	10.8	170
132	An Oxygenâ€Vacancyâ€Rich Semiconductorâ€5upported Bifunctional Catalyst for Efficient and Stable Zinc–Air Batteries. Advanced Materials, 2019, 31, e1806761.	11.1	133
133	Bimetallic synergy in cobalt–palladium nanocatalysts for CO oxidation. Nature Catalysis, 2019, 2, 78-85.	16.1	195
134	Methyl modified SiO2 aerogel with tailored dual modal pore structure for adsorption of organic solvents. Materials Letters, 2019, 238, 202-205.	1.3	24
135	Ultrathin Visibleâ€Lightâ€Driven Mo Incorporating In ₂ O ₃ –ZnIn ₂ Se ₄ Z cheme Nanosheet Photocatalysts. Advanced Materials, 2019, 31, e1807226.	11.1	165
136	Elucidating anionic oxygen activity in lithium-rich layered oxides. Nature Communications, 2018, 9, 947.	5.8	241
137	High acid resistant SiOC ceramic membranes for wastewater treatment. Ceramics International, 2018, 44, 13444-13448.	2.3	17
138	Nanoceria-Supported Single-Atom Platinum Catalysts for Direct Methane Conversion. ACS Catalysis, 2018, 8, 4044-4048.	5.5	214
139	Multistep Lithiation of Tin Sulfide: An Investigation Using <i>in Situ</i> Electron Microscopy. ACS Nano, 2018, 12, 3638-3645.	7.3	50
140	Core–shell PdPb@Pd aerogels with multiply-twinned intermetallic nanostructures: facile synthesis with accelerated gelation kinetics and their enhanced electrocatalytic properties. Journal of Materials Chemistry A, 2018, 6, 7517-7521.	5.2	49
141	A new strategy to synthesize anisotropic SmCo ₅ nanomagnets. Nanoscale, 2018, 10, 8735-8740.	2.8	37
142	SiOC nanolayer wrapped 3D interconnected graphene sponge as a high-performance anode for lithium ion batteries. Journal of Materials Chemistry A, 2018, 6, 9064-9073.	5.2	68
143	Interpenetrating Triphase Cobaltâ€Based Nanocomposites as Efficient Bifunctional Oxygen Electrocatalysts for Longâ€Lasting Rechargeable Zn–Air Batteries. Advanced Energy Materials, 2018, 8, 1702900.	10.2	242
144	Isolated Ni single atoms in graphene nanosheets for high-performance CO ₂ reduction. Energy and Environmental Science, 2018, 11, 893-903.	15.6	811

#	Article	IF	CITATIONS
145	Fe Stabilization by Intermetallic L1 ₀ -FePt and Pt Catalysis Enhancement in L1 ₀ -FePt/Pt Nanoparticles for Efficient Oxygen Reduction Reaction in Fuel Cells. Journal of the American Chemical Society, 2018, 140, 2926-2932.	6.6	312
146	Effect of Electrolyte on High Sulfur Loading Li-S Batteries. Journal of the Electrochemical Society, 2018, 165, A416-A423.	1.3	28
147	Porous Carbonâ€Hosted Atomically Dispersed Iron–Nitrogen Moiety as Enhanced Electrocatalysts for Oxygen Reduction Reaction in a Wide Range of pH. Small, 2018, 14, e1703118.	5.2	117
148	Coupled s-p-d Exchange in Facet-Controlled Pd3Pb Tripods Enhances Oxygen Reduction Catalysis. CheM, 2018, 4, 359-371.	5.8	100
149	Nitrogenâ€Coordinated Single Cobalt Atom Catalysts for Oxygen Reduction in Proton Exchange Membrane Fuel Cells. Advanced Materials, 2018, 30, 1706758.	11.1	788
150	Kern‣chale‣trukturierung rein metallischer Aerogele für eine hocheffiziente Nutzung von Platin für die Sauerstoffreduktion. Angewandte Chemie, 2018, 130, 3014-3018.	1.6	7
151	Core–Shell Structuring of Pure Metallic Aerogels towards Highly Efficient Platinum Utilization for the Oxygen Reduction Reaction. Angewandte Chemie - International Edition, 2018, 57, 2963-2966.	7.2	154
152	Superelastic and superhydrophobic bacterial cellulose/silica aerogels with hierarchical cellular structure for oil absorption and recovery. Journal of Hazardous Materials, 2018, 346, 199-207.	6.5	165
153	Large-scale and ultra-low thermal conductivity of ZrO2 fibrofelt/ZrO2-SiO2 aerogels composites for thermal insulation. Ceramics International, 2018, 44, 8742-8748.	2.3	41
154	Hydrothermal growth of 3D graphene on nickel foam as a substrate of nickel-cobalt-sulfur for high-performance supercapacitors. Journal of Alloys and Compounds, 2018, 732, 613-623.	2.8	36
155	Dislocation nucleation facilitated by atomicÂsegregation. Nature Materials, 2018, 17, 56-63.	13.3	99
156	Metal-organic frameworks derived platinum-cobalt bimetallic nanoparticles in nitrogen-doped hollow porous carbon capsules as a highly active and durable catalyst for oxygen reduction reaction. Applied Catalysis B: Environmental, 2018, 225, 496-503.	10.8	131
157	Biphase Cobalt–Manganese Oxide with High Capacity and Rate Performance for Aqueous Sodiumâ€lon Electrochemical Energy Storage. Advanced Functional Materials, 2018, 28, 1703266.	7.8	25
158	Panoramic Visualization of Lithiation of Copper Sulfide by In Situ STEM. Microscopy and Microanalysis, 2018, 24, 1498-1499.	0.2	1
159	Favorable Core/Shell Interface within Co ₂ P/Pt Nanorods for Oxygen Reduction Electrocatalysis. Nano Letters, 2018, 18, 7870-7875.	4.5	68
160	Crystallization kinetics and thermal stability of ZrO2 monolithic aerogel improved by SiO2 layer. Integrated Ferroelectrics, 2018, 191, 145-150.	0.3	1
161	Highly Dispersed Carbon Supported PdNiMo Core with Pt Monolayer Shell Electrocatalysts for Oxygen Reduction Reaction. Journal of the Electrochemical Society, 2018, 165, J3295-J3300.	1.3	8
162	Zeolite-Encapsulated Pt Nanoparticles for Tandem Catalysis. Journal of the American Chemical Society, 2018, 140, 13514-13520.	6.6	174

#	Article	IF	CITATIONS
163	Improvement of Li-S battery electrochemical performance with 2D TiS2 additive. Electrochimica Acta, 2018, 292, 779-788.	2.6	29
164	Correlating the electrocatalytic stability of platinum monolayer catalysts with their structural evolution in the oxygen reduction reaction. Journal of Materials Chemistry A, 2018, 6, 20725-20736.	5.2	22
165	In-situ Investigation of Multi-Step Lithiation of Tin Sulfide. Microscopy and Microanalysis, 2018, 24, 1864-1865.	0.2	0
166	Atomically dispersed manganese catalysts for oxygen reduction in proton-exchange membrane fuel cells. Nature Catalysis, 2018, 1, 935-945.	16.1	1,075
167	Pt alloy nanoparticles decorated on large-size nitrogen-doped graphene tubes for highly stable oxygen-reduction catalysts. Nanoscale, 2018, 10, 17318-17326.	2.8	45
168	In Situ Characterization of Cu/CeO ₂ Nanocatalysts for CO ₂ Hydrogenation: Morphological Effects of Nanostructured Ceria on the Catalytic Activity. Journal of Physical Chemistry C, 2018, 122, 12934-12943.	1.5	145
169	Tuning metal-insulator behavior in LaTiO3/SrTiO3 heterostructures integrated directly on Si(100) through control of atomic layer thickness. Applied Physics Letters, 2018, 112, .	1.5	9
170	Highly active subnanometer Rh clusters derived from Rh-doped SrTiO3 for CO2 reduction. Applied Catalysis B: Environmental, 2018, 237, 1003-1011.	10.8	67
171	Active sites for tandem reactions of CO ₂ reduction and ethane dehydrogenation. Proceedings of the National Academy of Sciences of the United States of America, 2018, 115, 8278-8283.	3.3	105
172	Nanovoid Incorporated Ir _{<i>x</i>} Cu Metallic Aerogels for Oxygen Evolution Reaction Catalysis. ACS Energy Letters, 2018, 3, 2038-2044.	8.8	129
173	Reversible Flat to Rippling Phase Transition in Fe Containing Layered Battery Electrode Materials. Advanced Functional Materials, 2018, 28, 1803896.	7.8	18
174	Superconducting epitaxial \$\$hbox {YBa}_{2}hbox {Cu}_{3}hbox {O}_{7-delta }\$\$ YBa 2 Cu 3 O 7. Bulletin of Materials Science, 2018, 41, 1.	0.8	1
175	Hierarchically Porous M–N–C (M = Co and Fe) Singleâ€Atom Electrocatalysts with Robust MN <i>_x</i> Active Moieties Enable Enhanced ORR Performance. Advanced Energy Materials, 2018, 8, 1801956.	10.2	540
176	Ultrafine Pd ensembles anchored-Au2Cu aerogels boost ethanol electrooxidation. Nano Energy, 2018, 53, 206-212.	8.2	54
177	Ordered Pt ₃ Co Intermetallic Nanoparticles Derived from Metal–Organic Frameworks for Oxygen Reduction. Nano Letters, 2018, 18, 4163-4171.	4.5	304
178	Zn-air Batteries: Interpenetrating Triphase Cobalt-Based Nanocomposites as Efficient Bifunctional Oxygen Electrocatalysts for Long-Lasting Rechargeable Zn-Air Batteries (Adv. Energy Mater. 15/2018). Advanced Energy Materials, 2018, 8, 1870068.	10.2	13
179	High energy-density and reversibility of iron fluoride cathode enabled via an intercalation-extrusion reaction. Nature Communications, 2018, 9, 2324.	5.8	136
180	Avoiding Fracture in a Conversion Battery Material through Reaction with Larger Ions. Joule, 2018, 2, 1783-1799.	11.7	65

#	Article	IF	CITATIONS
181	Reversible Flat to Rippling Phase Transition in Fe Containing Layered Battery Electrode Materials. Advanced Functional Materials, 2018, 28, .	7.8	Ο
182	Electrically coupling complex oxides to semiconductors: A route to novel material functionalities. Journal of Materials Research, 2017, 32, 249-259.	1.2	14
183	CuNi Nanoparticles Assembled on Graphene for Catalytic Methanolysis of Ammonia Borane and Hydrogenation of Nitro/Nitrile Compounds. Chemistry of Materials, 2017, 29, 1413-1418.	3.2	149
184	Gradient structure high emissivity MoSi2-SiO2-SiOC coating forÂthermal protective application. Journal of Alloys and Compounds, 2017, 703, 437-447.	2.8	36
185	Core–shell-structured Li ₃ V ₂ (PO ₄) ₃ –LiVOPO ₄ nanocomposites cathode for high-rate and long-life lithium-ion batteries. RSC Advances, 2017, 7, 3101-3107.	1.7	9
186	NixWO2.72 nanorods as an efficient electrocatalyst for oxygen evolution reaction. Green Energy and Environment, 2017, 2, 119-123.	4.7	15
187	Advanced electron microscopy characterization of nanomaterials for catalysis. Green Energy and Environment, 2017, 2, 70-83.	4.7	97
188	Flexible Heteroepitaxy of CoFe ₂ O ₄ /Muscovite Bimorph with Large Magnetostriction. ACS Applied Materials & Interfaces, 2017, 9, 7297-7304.	4.0	108
189	Selfâ€Assembled Fe–Nâ€Doped Carbon Nanotube Aerogels with Singleâ€Atom Catalyst Feature as Highâ€Efficiency Oxygen Reduction Electrocatalysts. Small, 2017, 13, 1603407.	5.2	254
190	Bifunctional Ag@SiO 2 /Au Nanoparticles for Probing Sequential Catalytic Reactions by Surfaceâ€Enhanced Raman Spectroscopy. ChemNanoMat, 2017, 3, 245-251.	1.5	10
191	Fabrication and toughening behavior of carbon nanotube (CNT) scaffold reinforced SiBCN ceramic composites with high CNT loading. Ceramics International, 2017, 43, 9024-9031.	2.3	22
192	Interaction of TiS ₂ and Sulfur in Li-S Battery System. Journal of the Electrochemical Society, 2017, 164, A1291-A1297.	1.3	60
193	Structural Evolution of Sub-10 nm Octahedral Platinum–Nickel Bimetallic Nanocrystals. Nano Letters, 2017, 17, 3926-3931.	4.5	57
194	Strain Coupling of Conversionâ€ŧype Fe ₃ O ₄ Thin Films for Lithium Ion Batteries. Angewandte Chemie - International Edition, 2017, 56, 7813-7816.	7.2	59
195	Strain Coupling of Conversionâ€ŧype Fe 3 O 4 Thin Films for Lithium Ion Batteries. Angewandte Chemie, 2017, 129, 7921-7924.	1.6	2
196	Surface Proton Transfer Promotes Four-Electron Oxygen Reduction on Gold Nanocrystal Surfaces in Alkaline Solution. Journal of the American Chemical Society, 2017, 139, 7310-7317.	6.6	51
197	Hard–Soft Composite Carbon as a Long ycling and Highâ€Rate Anode for Potassiumâ€Ion Batteries. Advanced Functional Materials, 2017, 27, 1700324.	7.8	471
198	Atomic scale deposition of Pt around Au nanoparticles to achieve much enhanced electrocatalysis of Pt. Nanoscale, 2017, 9, 7745-7749.	2.8	24

#	Article	IF	CITATIONS
199	Epitaxial corundum-VTiO3 thin films grown on c-cut sapphire. Thin Solid Films, 2017, 631, 85-92.	0.8	5
200	Flexible Multiferroic Bulk Heterojunction with Giant Magnetoelectric Coupling <i>via</i> van der Waals Epitaxy. ACS Nano, 2017, 11, 6122-6130.	7.3	118
201	Effects of proton irradiation on structural and electrochemical charge storage properties of TiO ₂ nanotube electrodes for lithium-ion batteries. Journal of Materials Chemistry A, 2017, 5, 11815-11824.	5.2	45
202	Pt-based catalysts with tensile surface strain to boost activity. Fuel Cells Bulletin, 2017, 2017, 14.	0.7	0
203	Effect of Carbon and Binder on High Sulfur Loading Electrode for Li-S Battery Technology. Electrochimica Acta, 2017, 235, 399-408.	2.6	32
204	Quaternary FeCoNiMn-Based Nanocarbon Electrocatalysts for Bifunctional Oxygen Reduction and Evolution: Promotional Role of Mn Doping in Stabilizing Carbon. ACS Catalysis, 2017, 7, 8386-8393.	5.5	131
205	Stabilizing CuPd Nanoparticles via CuPd Coupling to WO _{2.72} Nanorods in Electrochemical Oxidation of Formic Acid. Journal of the American Chemical Society, 2017, 139, 15191-15196.	6.6	106
206	Local electric field direct writing – Electron-beam lithography and mechanism. Microelectronic Engineering, 2017, 182, 8-14.	1.1	1
207	Single Atomic Iron Catalysts for Oxygen Reduction in Acidic Media: Particle Size Control and Thermal Activation. Journal of the American Chemical Society, 2017, 139, 14143-14149.	6.6	1,215
208	3D polymer hydrogel for high-performance atomic iron-rich catalysts for oxygen reduction in acidic media. Applied Catalysis B: Environmental, 2017, 219, 629-639.	10.8	111
209	Kinetically-Driven Phase Transformation during Lithiation in Copper Sulfide Nanoflakes. Nano Letters, 2017, 17, 5726-5733.	4.5	67
210	Improvement of thermal stability of ZrO2–SiO2 aerogels by an inorganic–organic synergetic surface modification. Journal of Porous Materials, 2017, 24, 657-665.	1.3	13
211	Interaction of FeS ₂ and Sulfur in Li-S Battery System. Journal of the Electrochemical Society, 2017, 164, A6039-A6046.	1.3	46
212	Morphology Control of Carbon-Free Spinel NiCo ₂ O ₄ Catalysts for Enhanced Bifunctional Oxygen Reduction and Evolution in Alkaline Media. ACS Applied Materials & Interfaces, 2017, 9, 44567-44578.	4.0	161
213	Development of Real-Time Probe Current Calibration for Performing Quantitative STEM with a Cold Field-Emission Gun Microscopy and Microanalysis, 2016, 22, 940-941.	0.2	0
214	Direct Visualization of Lithium Intercalation in Spinel Iron Oxide by In-Situ Bright-Field Scanning Transmission Electron Microscopy. Microscopy and Microanalysis, 2016, 22, 760-761.	0.2	1
215	Ordered PdCuâ€Based Nanoparticles as Bifunctional Oxygenâ€Reduction and Ethanolâ€Oxidation Electrocatalysts. Angewandte Chemie, 2016, 128, 9176-9181.	1.6	56
216	Ordered PdCuâ€Based Nanoparticles as Bifunctional Oxygenâ€Reduction and Ethanolâ€Oxidation Electrocatalysts. Angewandte Chemie - International Edition, 2016, 55, 9030-9035.	7.2	278

#	Article	IF	CITATIONS
217	Polyvinylpyrrolidone-induced anisotropic growth of gold nanoprisms in plasmon-driven synthesis. Nature Materials, 2016, 15, 889-895.	13.3	239
218	STEM/EELS Analysis of Li(Ni 0.8 Co 0.15 Al 0.05)O 2 Held at High Voltages. Microscopy and Microanalysis, 2016, 22, 1306-1307.	0.2	1
219	Visualizing non-equilibrium lithiation of spinel oxide via in situ transmission electron microscopy. Nature Communications, 2016, 7, 11441.	5.8	162
220	Biaxially strained PtPb/Pt core/shell nanoplate boosts oxygen reduction catalysis. Science, 2016, 354, 1410-1414.	6.0	1,262
221	Chemical strain-dependent two-dimensional transport at <mml:math xmlns:mml="http://www.w3.org/1998/Math/MathML"> <mml:mrow> <mml:mi>R</mml:mi> <mml:msub> <mml:m interfaces <mml:math< td=""><td>text>AlO<</td><td>/mml:mtext></td></mml:math<></mml:m </mml:msub></mml:mrow></mml:math 	text>AlO<	/mml:mtext>

#	Article	IF	CITATIONS
235	Surface engineering of hierarchical platinum-cobalt nanowires for efficient electrocatalysis. Nature Communications, 2016, 7, 11850.	5.8	607
236	Nanoscale Origins of Ferroelastic Domain Wall Mobility in Ferroelectric Multilayers. ACS Nano, 2016, 10, 10126-10134.	7.3	11
237	Controlling the Active Sites of Sulfurâ€Doped Carbon Nanotube–Graphene Nanolobes for Highly Efficient Oxygen Evolution and Reduction Catalysis. Advanced Energy Materials, 2016, 6, 1501966.	10.2	242
238	Sea urchin-like cobalt–iron phosphide as an active catalyst for oxygen evolution reaction. Nanoscale, 2016, 8, 3244-3247.	2.8	135
239	Ag@Au Concave Cuboctahedra: A Unique Probe for Monitoring Au-Catalyzed Reduction and Oxidation Reactions by Surface-Enhanced Raman Spectroscopy. ACS Nano, 2016, 10, 2607-2616.	7.3	125
240	Super-hydrophobic hexamethyl-disilazane modified ZrO ₂ –SiO ₂ aerogels with excellent thermal stability. Journal of Materials Chemistry A, 2016, 4, 5632-5638.	5.2	61
241	Ultra-low thermal conductivity and high strength of aerogels/fibrous ceramic composites. Journal of the European Ceramic Society, 2016, 36, 1487-1493.	2.8	140
242	Effect of glass phase content on structure and properties of gradient MoSi 2 –BaO–Al 2 O 3 –SiO 2 coating for porous fibrous insulations. Journal of Alloys and Compounds, 2016, 657, 684-690.	2.8	27
243	Preparation and characterization of continuous SiZrOC fibers by polyvinyl pyrrolidone-assisted sol–gel process. Journal of Materials Science, 2016, 51, 1418-1427.	1.7	23
244	Exchange bias effect in <mml:math xmlns:mml="http://www.w3.org/1998/Math/MathML"><mml:mrow><mml:msub><mml:mtext>Au-Femathvariant="normal">O<mml:mn>4</mml:mn></mml:mtext></mml:msub></mml:mrow>dumbbell nanoparticles induced by the charge transfer from gold. Physical Review B, 2015, 92, .</mml:math 	t> <mml:n 1.1</mml:n 	nn>3
245	Interfacial Structure in Epitaxial Perovskite Oxides on (001) Ge Crystal. Microscopy and Microanalysis, 2015, 21, 1301-1302.	0.2	Ο
246	Development of Quantitative STEM for a Conventional S/TEM and Real-Time Current Calibration for Performing QSTEM with a Cold Field Emission Gun. Microscopy and Microanalysis, 2015, 21, 2127-2128.	0.2	1
247	Comparison of Co3O4 and CoO Nanoparticles as Anodes for Lithium-ion Batteries. Microscopy and Microanalysis, 2015, 21, 477-478.	0.2	2
248	A General Method for Multimetallic Platinum Alloy Nanowires as Highly Active and Stable Oxygen Reduction Catalysts. Advanced Materials, 2015, 27, 7204-7212.	11.1	280
249	Controlled Anisotropic Growth of Coâ€Feâ€P from Coâ€Feâ€O Nanoparticles. Angewandte Chemie - International Edition, 2015, 54, 9642-9645.	7.2	132
250	Pt Monolayer Shell on Nitrided Alloy Core—A Path to Highly Stable Oxygen Reduction Catalyst. Catalysts, 2015, 5, 1321-1332.	1.6	33
251	Contrasting Reaction Modality between Electrochemical Sodiation and Lithiation in NiO Conversion Electrode Materials. Microscopy and Microanalysis, 2015, 21, 325-326.	0.2	2
252	Revealing Near-Surface to Interior Redox upon Lithiation in Conversion Electrode Materials Using Electron Microscopy. Microscopy and Microanalysis, 2015, 21, 1369-1370.	0.2	0

#	Article	IF	CITATIONS
253	Investigation of the Structural and Electronic Properties of Pt/γ-Al2O3, a Model Catalyst System. Microscopy and Microanalysis, 2015, 21, 1655-1656.	0.2	0
254	EELS Analysis Of Lithiation/Delithiation Reactions In LiFePO4. Microscopy and Microanalysis, 2015, 21, 331-332.	0.2	0
255	Shape-Controlled Narrow-Gap SnTe Nanostructures: From Nanocubes to Nanorods and Nanowires. Journal of the American Chemical Society, 2015, 137, 15074-15077.	6.6	42
256	Ultrathin and stable AgAu alloy nanowires. Science China Materials, 2015, 58, 595-602.	3.5	13
257	Exceptional activity of sub-nm Pt clusters on CdS for photocatalytic hydrogen production: a combined experimental and first-principles study. Catalysis Science and Technology, 2015, 5, 2059-2064.	2.1	26
258	Strain and Stability of Ultrathin Ge Layers in Si/Ge/Si Axial Heterojunction Nanowires. Nano Letters, 2015, 15, 1654-1659.	4.5	24
259	Transitions from Near-Surface to Interior Redox upon Lithiation in Conversion Electrode Materials. Nano Letters, 2015, 15, 1437-1444.	4.5	97
260	Bandâ€Gap Engineering at a Semiconductor–Crystalline Oxide Interface. Advanced Materials Interfaces, 2015, 2, 1400497.	1.9	31
261	New Approach to Fully Ordered fct-FePt Nanoparticles for Much Enhanced Electrocatalysis in Acid. Nano Letters, 2015, 15, 2468-2473.	4.5	385
262	Ultra-high-performance core–shell structured Ru@Pt/C catalyst prepared by a facile pulse electrochemical deposition method. Scientific Reports, 2015, 5, 11604.	1.6	21
263	Constructing Hierarchical Interfaces: TiO ₂ -Supported PtFe–FeO _{<i>x</i>} Nanowires for Room Temperature CO Oxidation. Journal of the American Chemical Society, 2015, 137, 10156-10159.	6.6	86
264	Synthesis and X-ray Characterization of Cobalt Phosphide (Co ₂ P) Nanorods for the Oxygen Reduction Reaction. ACS Nano, 2015, 9, 8108-8115.	7.3	132
265	Enhancement of the oxygen reduction on nitride stabilized pt-M (M=Fe, Co, and Ni) core–shell nanoparticle electrocatalysts. Nano Energy, 2015, 13, 442-449.	8.2	104
266	Characterization of V-shaped Defects in 4H-SiC Homoepitaxial Layers. Journal of Electronic Materials, 2015, 44, 1293-1299.	1.0	4
267	Continuous sol–gel derived SiOC/HfO ₂ fibers with high strength. RSC Advances, 2015, 5, 35026-35032.	1.7	17
268	LaTiO3/KTaO3 interfaces: A new two-dimensional electron gas system. APL Materials, 2015, 3, .	2.2	94
269	Ternary metal fluorides as high-energy cathodes with low cycling hysteresis. Nature Communications, 2015, 6, 6668.	5.8	138
270	Surface Profile Control of FeNiPt/Pt Core/Shell Nanowires for Oxygen Reduction Reaction. Small, 2015, 11, 3545-3549.	5.2	61

#	Article	IF	CITATIONS
271	Preparation of SiOC/HfO2 fibers from silicon alkoxides and tetrachloride hafnium by a sol–gel process. Materials Letters, 2015, 148, 196-199.	1.3	16
272	Enhancing grain boundary ionic conductivity in mixed ionic–electronic conductors. Nature Communications, 2015, 6, 6824.	5.8	195
273	High-strength mullite fibers reinforced ZrO2–SiO2 aerogels fabricated by rapid gel method. Journal of Materials Science, 2015, 50, 7488-7494.	1.7	50
274	In Situ Probing of the Active Site Geometry of Ultrathin Nanowires for the Oxygen Reduction Reaction. Journal of the American Chemical Society, 2015, 137, 12597-12609.	6.6	46
275	Interaction of CuS and Sulfur in Li-S Battery System. Journal of the Electrochemical Society, 2015, 162, A2834-A2839.	1.3	62
276	Interfacial structure in epitaxial perovskite oxides on (001) Ge crystal. Applied Physics Letters, 2015, 106, .	1.5	11
277	Structure Stabilization by Mixed Anions in Oxyfluoride Cathodes for High-Energy Lithium Batteries. ACS Nano, 2015, 9, 10076-10084.	7.3	54
278	Sodiation Kinetics of Metal Oxide Conversion Electrodes: A Comparative Study with Lithiation. Nano Letters, 2015, 15, 5755-5763.	4.5	122
279	Phase separation induced macroporous SiOC ceramics derived from polysiloxane. Journal of the European Ceramic Society, 2015, 35, 443-450.	2.8	29
280	Interfacial dislocations in (111) oriented (Ba0.7Sr0.3)TiO3films on SrTiO3single crystal. Applied Physics Letters, 2015, 107, 141605.	1.5	2
281	Core/Shell Au/MnO Nanoparticles Prepared Through Controlled Oxidation of AuMn as an Electrocatalyst for Sensitive H ₂ O ₂ Detection. Angewandte Chemie - International Edition, 2014, 53, 12508-12512.	7.2	84
282	Comparative study of the alloying effect on the initial oxidation of Cu-Au(100) and Cu-Pt(100). Applied Physics Letters, 2014, 104, 121601.	1.5	15
283	Gallium Sulfide–Singleâ€Walled Carbon Nanotube Composites: Highâ€Performance Anodes for Lithiumâ€lon Batteries. Advanced Functional Materials, 2014, 24, 5435-5442.	7.8	102
284	TEM Characterization of Metallic Nanocatalysts. , 2014, , 577-618.		1
285	Heterojunction nanowires having high activity and stability for the reduction of oxygen: Formation by self-assembly of iron phthalocyanine with single walled carbon nanotubes (FePc/SWNTs). Journal of Colloid and Interface Science, 2014, 419, 61-67.	5.0	24
286	Metalizing carbon nanotubes with Pd–Pt core–shell nanowires enhances electrocatalytic activity and stability in the oxygen reduction reaction. Journal of Solid State Electrochemistry, 2014, 18, 1171-1179.	1.2	19
287	Direct visualization of the Jahn–Teller effect coupled to Na ordering in Na5/8MnO2. Nature Materials, 2014, 13, 586-592.	13.3	237
288	Investigation of Changes in the Surface Structure of Li _{<i>x</i>} Ni _{0.8} Co _{0.15} Al _{0.05} O ₂ Cathode Materials Induced by the Initial Charge. Chemistry of Materials, 2014, 26, 1084-1092.	3.2	308

#	Article	IF	CITATIONS
289	The role of transition metals in the catalytic activity of Pt alloys: quantification of strain and ligand effects. Chemical Communications, 2014, 50, 2173.	2.2	58
290	High Performance Pt Monolayer Catalysts Produced via Core-Catalyzed Coating in Ethanol. ACS Catalysis, 2014, 4, 738-742.	5.5	78
291	Unlocking the Potential of Cation-Disordered Oxides for Rechargeable Lithium Batteries. Science, 2014, 343, 519-522.	6.0	943
292	Gold-promoted structurally ordered intermetallic palladium cobalt nanoparticles for the oxygen reduction reaction. Nature Communications, 2014, 5, 5185.	5.8	134
293	Monodisperse Core/Shell Ni/FePt Nanoparticles and Their Conversion to Ni/Pt to Catalyze Oxygen Reduction. Journal of the American Chemical Society, 2014, 136, 15921-15924.	6.6	165
294	A facile route to monodisperse MPd (M = Co or Cu) alloy nanoparticles and their catalysis for electrooxidation of formic acid. Nanoscale, 2014, 6, 6970-6973.	2.8	92
295	Influence of crystal structure on the electrochemical performance of A-site-deficient Sr _{1â^'s} Nb _{0.1} Co _{0.9} O _{3â^'l´} perovskite cathodes. RSC Advances, 2014, 4, 40865-40872.	1.7	40
296	Characterization of 3D interconnected microstructural network in mixed ionic and electronic conducting ceramic composites. Nanoscale, 2014, 6, 4480.	2.8	19
297	Synthesis and Characterization of Ethyleneâ€Bridged Copolycarbosilazane as Precursors for Silicon Carbonitride Ceramics. Journal of the American Ceramic Society, 2014, 97, 1311-1316.	1.9	17
298	Sodiation <i>via</i> Heterogeneous Disproportionation in FeF ₂ Electrodes for Sodium-Ion Batteries. ACS Nano, 2014, 8, 7251-7259.	7.3	89
299	Direct-methane solid oxide fuel cells with hierarchically porous Ni-based anode deposited with nanocatalyst layer. Nano Energy, 2014, 10, 1-9.	8.2	100
300	Remarkably Improved Electrode Performance of Bulk MnS by Forming a Solid Solution with FeS – Understanding the Li Storage Mechanism. Advanced Functional Materials, 2014, 24, 5557-5566.	7.8	49
301	Electronic structure of cobalt doped CdSe quantum dots using soft X-ray spectroscopy. Journal of Materials Chemistry C, 2014, 2, 8313-8321.	2.7	4
302	Platinum-Tin Oxide Core–Shell Catalysts for Efficient Electro-Oxidation of Ethanol. Journal of the American Chemical Society, 2014, 136, 10862-10865.	6.6	180
303	Determining the Resolution Limits of Electron-Beam Lithography: Direct Measurement of the Point-Spread Function. Nano Letters, 2014, 14, 4406-4412.	4.5	67
304	Surface Plasmon-Driven Water Reduction: Gold Nanoparticle Size Matters. Journal of the American Chemical Society, 2014, 136, 9842-9845.	6.6	301
305	Nanocatalyst Superior to Pt for Oxygen Reduction Reactions: The Case of Core/Shell Ag(Au)/CuPd Nanoparticles. Journal of the American Chemical Society, 2014, 136, 15026-15033.	6.6	172
306	Core–shell, hollow-structured iridium–nickel nitride nanoparticles for the hydrogen evolution reaction. Journal of Materials Chemistry A, 2014, 2, 591-594.	5.2	83

#	Article	IF	CITATIONS
307	Evaluation of Li2O as an efficient sintering aid for gadolinia-doped ceria electrolyte for solid oxide fuel cells. Journal of Power Sources, 2014, 261, 255-263.	4.0	72
308	Prolonged Hot Electron Dynamics in Plasmonicâ€Metal/Semiconductor Heterostructures with Implications for Solar Photocatalysis. Angewandte Chemie - International Edition, 2014, 53, 7887-7891.	7.2	349
309	Tuning Nanoparticle Structure and Surface Strain for Catalysis Optimization. Journal of the American Chemical Society, 2014, 136, 7734-7739.	6.6	349
310	Low temperature solid oxide fuel cells with hierarchically porous cathode nano-network. Nano Energy, 2014, 8, 25-33.	8.2	144
311	Probing the Local Chemical and Structural Ordering of Iron Oxyfluoride. Microscopy and Microanalysis, 2014, 20, 430-431.	0.2	0
312	Discovering a Novel Sodiation in FeF2 Electrodes for Sodium-Ion Batteries. Microscopy and Microanalysis, 2014, 20, 490-491.	0.2	1
313	A Model Based Method for Tomographic Reconstructions of Nanoparticle Assemblies. Microscopy and Microanalysis, 2014, 20, 808-809.	0.2	1
314	10.1063/1.4870085.1., 2014, , .		1
315	Pt monolayer on Au-stabilized PdNi core–shell nanoparticles for oxygen reduction reaction. Electrochimica Acta, 2013, 110, 267-272.	2.6	70
316	Highly Ordered TiO ₂ Nanotubes on Patterned Substrates: Synthesis-in-Place for Ultrasensitive Chemiresistors. Journal of Physical Chemistry C, 2013, 117, 17824-17831.	1.5	24
317	Core–shell catalysts consisting of nanoporous cores for oxygen reduction reaction. Physical Chemistry Chemical Physics, 2013, 15, 15078.	1.3	32
318	Seed-Mediated Synthesis of Core/Shell FePtM/FePt (M = Pd, Au) Nanowires and Their Electrocatalysis for Oxygen Reduction Reaction. Journal of the American Chemical Society, 2013, 135, 13879-13884.	6.6	269
319	Manipulating the oxygen reduction activity of platinum shells with shape-controlled palladium nanocrystal cores. Chemical Communications, 2013, 49, 9030.	2.2	62
320	Ordered bilayer ruthenium–platinum core-shell nanoparticles as carbon monoxide-tolerant fuel cell catalysts. Nature Communications, 2013, 4, 2466.	5.8	200
321	Structural phase transformation and Fe valence evolution in FeOxF2â^'x/C nanocomposite electrodes during lithiation and de-lithiation processes. Journal of Materials Chemistry A, 2013, 1, 11629.	5.2	49
322	Excess lithium storage and charge compensation in nanoscale Li _{4+<i>x</i>} Ti ₅ O ₁₂ . Nanotechnology, 2013, 24, 424006.	1.3	37
323	The first experimental demonstration of beneficial effects of sub-nanometer platinum particles for photocatalysis. Chemical Engineering Journal, 2013, 217, 266-272.	6.6	6
324	Resolution Limits of Electron-Beam Lithography toward the Atomic Scale. Nano Letters, 2013, 13, 1555-1558.	4.5	350

#	Article	IF	CITATIONS
325	Monodisperse AgPd Alloy Nanoparticles and Their Superior Catalysis for the Dehydrogenation of Formic Acid. Angewandte Chemie - International Edition, 2013, 52, 3681-3684.	7.2	348
326	Synthetic Control of FePtM Nanorods (M = Cu, Ni) To Enhance the Oxygen Reduction Reaction. Journal of the American Chemical Society, 2013, 135, 7130-7133.	6.6	250
327	Origin of Phonon Glass–Electron Crystal Behavior in Thermoelectric Layered Cobaltate. Advanced Functional Materials, 2013, 23, 5728-5736.	7.8	47
328	Engineering nano-composite Li4Ti5O12 anodes via scanning electron-probe fabrication. Nano Energy, 2013, 2, 343-350.	8.2	40
329	Discrete Nanocubes as Plasmonic Reporters of Molecular Chirality. Nano Letters, 2013, 13, 3145-3151.	4.5	178
330	Pseudocapacitive Hausmannite Nanoparticles with (101) Facets: Synthesis, Characterization, and Chargeâ€Iransfer Mechanism. ChemSusChem, 2013, 6, 1983-1992.	3.6	22
331	Reactive ion etching: Optimized diamond membrane fabrication for transmission electron microscopy. Journal of Vacuum Science and Technology B:Nanotechnology and Microelectronics, 2013, 31, 06FF01.	0.6	14
332	Storage of Potassium Ions in Layered Vanadium Pentoxide Nanofiber Electrodes for Aqueous Pseudocapacitors. ChemSusChem, 2013, 6, 2231-2235.	3.6	16
333	Interfacial reconstruction and superconductivity in cuprate–manganite multilayers of YBa ₂ Cu ₃ O _{7â^'<i>δ</i>} and Pr _{0.68} Ca _{0.32} MnO ₃ . New Journal of Physics, 2012, 14, 093009.	1.2	4
334	Electron-Beam-Induced Structure transition in spinel Li4Ti5O12. Microscopy and Microanalysis, 2012, 18, 1488-1489.	0.2	1
335	High-resolution characterization of activated graphene for supercapacitor applications. Microscopy and Microanalysis, 2012, 18, 1536-1537.	0.2	0
336	Controlling the Particle Size of ZrO ₂ Nanoparticles in Hydrothermally Stable ZrO ₂ /MWCNT Composites. Langmuir, 2012, 28, 17159-17167.	1.6	17
337	Palladium–Tin Alloyed Catalysts for the Ethanol Oxidation Reaction in an Alkaline Medium. ACS Catalysis, 2012, 2, 287-297.	5.5	266
338	Pseudocapacitive NiO Fine Nanoparticles for Supercapacitor Reactions. Journal of the Electrochemical Society, 2012, 159, A1598-A1603.	1.3	44
339	Outstanding activity of sub-nm Au clusters for photocatalytic hydrogen production. Applied Catalysis B: Environmental, 2012, 126, 153-160.	10.8	48
340	Do Eu dopants prefer the precipitated LaF ₃ nanocrystals in glass ceramics?. Physica Status Solidi - Rapid Research Letters, 2012, 6, 487-489.	1.2	18
341	Structure-Induced Enhancement in Electrooxidation of Trimetallic FePtAu Nanoparticles. Journal of the American Chemical Society, 2012, 134, 5060-5063.	6.6	185
342	Nitride Stabilized PtNi Core–Shell Nanocatalyst for high Oxygen Reduction Activity. Nano Letters, 2012, 12, 6266-6271.	4.5	213

#	Article	IF	CITATIONS
343	Iridium–Ruthenium Alloyed Nanoparticles for the Ethanol Oxidation Fuel Cell Reactions. ACS Catalysis, 2012, 2, 1226-1231.	5.5	47
344	Synthesis and Characterization of Nanocomposites with Strong Interfacial Interaction: Sulfated ZrO ₂ Nanoparticles Supported on Multiwalled Carbon Nanotubes. Journal of Physical Chemistry C, 2012, 116, 21742-21752.	1.5	33
345	Polaron absorption for photovoltaic energy conversion in a manganite-titanate <mml:math xmlns:mml="http://www.w3.org/1998/Math/MathML" display="inline"><mml:mrow><mml:mi mathvariant="bold-italic">pn</mml:mi </mml:mrow>heterojunction. Physical Review B, 2012. 85</mml:math 	1.1	28
346	Tetrahedral Palladium Nanocrystals: AÂNew Support for Platinum Monolayer Electrocatalysts with High Activity and Stability in the Oxygen Reduction Reaction. Zeitschrift Fur Physikalische Chemie, 2012, 226, 1025-1038.	1.4	15
347	Highly Efficient K _{0.15} MnO ₂ Birnessite Nanosheets for Stable Pseudocapacitive Cathodes. Journal of Physical Chemistry C, 2012, 116, 20173-20181.	1.5	65
348	Bimetallic IrNi core platinum monolayer shell electrocatalysts for the oxygen reduction reaction. Energy and Environmental Science, 2012, 5, 5297-5304.	15.6	156
349	Highly Active Pt ₃ Pb and Core–Shell Pt ₃ Pb–Pt Electrocatalysts for Formic Acid Oxidation. ACS Nano, 2012, 6, 2818-2825.	7.3	177
350	Electrooxidation of Methanol at SnO _{<i>x</i>} –Pt Interface: A Tunable Activity of Tin Oxide Nanoparticles. Journal of Physical Chemistry Letters, 2012, 3, 3286-3290.	2.1	44
351	Controlling the Growth of Si/Ge Nanowires and Heterojunctions Using Silver–Gold Alloy Catalysts. ACS Nano, 2012, 6, 6407-6415.	7.3	77
352	Fe valence determination and Li elemental distribution in lithiated FeO0.7F1.3/C nanocomposite battery materials by electron energy loss spectroscopy (EELS). Micron, 2012, 43, 22-29.	1.1	70
353	Carbon-Supported IrNi Core–Shell Nanoparticles: Synthesis, Characterization, and Catalytic Activity. Journal of Physical Chemistry C, 2011, 115, 9894-9902.	1.5	58
354	Strong growth orientation dependence of strain relaxation in epitaxial (Ba,Sr)TiO3 films and the resulting dielectric properties. Journal of Applied Physics, 2011, 109, .	1.1	24
355	Promotional Effects of Bismuth on the Formation of Platinumâ^Bismuth Nanowires Network and the Electrocatalytic Activity toward Ethanol Oxidation. Crystal Growth and Design, 2011, 11, 594-599.	1.4	36
356	Highly Active Iridium/Iridium–Tin/Tin Oxide Heterogeneous Nanoparticles as Alternative Electrocatalysts for the Ethanol Oxidation Reaction. Journal of the American Chemical Society, 2011, 133, 15172-15183.	6.6	167
357	The interaction of electromagnetic wave and plasma wave in an electron beam-ion channel system. Physics of Plasmas, 2011, 18, .	0.7	23
358	Embossed TiO ₂ Thin Films with Tailored Links between Hollow Hemispheres: Synthesis and Gas-Sensing Properties. Journal of Physical Chemistry C, 2011, 115, 9993-9999.	1.5	42
359	Ternary PtSnRh–SnO2 nanoclusters: synthesis and electroactivity for ethanol oxidation fuel cell reaction. Journal of Materials Chemistry, 2011, 21, 8887.	6.7	64
360	Kirkendall Effect and Lattice Contraction in Nanocatalysts: A New Strategy to Enhance Sustainable Activity. Journal of the American Chemical Society, 2011, 133, 13551-13557.	6.6	255

#	Article	IF	CITATIONS
361	Metallic and Insulating Oxide Interfaces Controlled by Electronic Correlations. Science, 2011, 331, 886-889.	6.0	212
362	Oxide Surface Crystallography in Electron Microscopy. Microscopy and Microanalysis, 2011, 17, 1084-1085.	0.2	0
363	Domain Pinning and Valence State Switching in Pb(Zr0.2Ti0.8)O3/La0.8Sr0.2MnO3 Heterostructures. Microscopy and Microanalysis, 2011, 17, 1400-1401.	0.2	0
364	Nanostructured electrodes for organic bulk heterojunction solar cells: Model study using carbon nanotube dispersed polythiophene-fullerene blend devices. Journal of Applied Physics, 2011, 110, .	1.1	17
365	Photocatalytic properties of TiO2 supported on SBA-15 mesoporous materials with large pores and short channels. Materials Letters, 2011, 65, 3354-3357.	1.3	18
366	Conversion Reaction Mechanisms in Lithium Ion Batteries: Study of the Binary Metal Fluoride Electrodes. Journal of the American Chemical Society, 2011, 133, 18828-18836.	6.6	492
367	Carbon-Based Supercapacitors Produced by Activation of Graphene. Science, 2011, 332, 1537-1541.	6.0	5,528
368	Experimental study of resistive bistability in metal oxide junctions. Applied Physics A: Materials Science and Processing, 2011, 103, 293-300.	1.1	0
369	Platinum Monolayer on IrFe Core–Shell Nanoparticle Electrocatalysts for the Oxygen Reduction Reaction. Electrocatalysis, 2011, 2, 134-140.	1.5	31
370	Novel photocatalytic applications of sub-nanometer gold particles for environmental liquid and gas phase reactions. Applied Catalysis B: Environmental, 2011, 104, 239-244.	10.8	18
371	Atomic imaging using secondary electrons in a scanning transmission electron microscope: Experimental observations and possible mechanisms. Ultramicroscopy, 2011, 111, 865-876.	0.8	65
372	Origin of 90° domain wall pinning in Pb(Zr _{0.2} Ti _{0.8})O ₃ heteroepitaxial thin films. Applied Physics Letters, 2011, 99, 102902.	1.5	49
373	Growth-mode induced defects in epitaxial SrTiO ₃ thin films grown on single crystal LaAlO ₃ by a two-step PLD process. Journal of Materials Research, 2011, 26, 770-774.	1.2	13
374	Ethanol oxidation on the ternary Pt–Rh–SnO2/C electrocatalysts with varied Pt:Rh:Sn ratios. Electrochimica Acta, 2010, 55, 4331-4338.	2.6	191
375	Scanning moiré fringe imaging by scanning transmission electron microscopy. Ultramicroscopy, 2010, 110, 229-233.	0.8	80
376	Fabrication of silicon oxycarbide fibers from alkoxide solutions along the sol–gel process. Journal of Sol-Gel Science and Technology, 2010, 56, 184-190.	1.1	24
377	Platinum-monolayer electrocatalysts: Palladium interlayer on IrCo alloy core improves activity in oxygen-reduction reaction. Journal of Electroanalytical Chemistry, 2010, 649, 232-237.	1.9	45
378	Pyrolytic transformation of liquid precursors to shaped bulk ceramics. Journal of the European Ceramic Society, 2010, 30, 1503-1511.	2.8	45

#	Article	IF	CITATIONS
379	On the measurement of thickness in nanoporous materials by EELS. Ultramicroscopy, 2010, 111, 62-65.	0.8	6
380	Microstructure and electronic behavior of PtPd@Pt core-shell nanowires. Journal of Materials Research, 2010, 25, 711-717.	1.2	7
381	Valence electron energy-loss spectroscopy of ultrathin SrTiO3 films grown on silicon (100) single crystal. Applied Physics Letters, 2010, 96, .	1.5	7
382	The atomic structure and polarization of strained SrTiO3/Si. Applied Physics Letters, 2010, 97, 251902.	1.5	25
383	Interface-Induced Polarization and Inhibition of Ferroelectricity in Epitaxial <mml:math xmlns:mml="http://www.w3.org/1998/Math/MathML" display="inline"><mml:msub><mml:mi>SrTiO</mml:mi><mml:mn>3</mml:mn></mml:msub><mml:mo>/Physical Review Letters, 2010, 105, 217601.</mml:mo></mml:math 	no>?mml:	:mi>Si
384	Electric field tuned crossover from classical to weakly localized quantum transport in electron doped <mml:math display="inline" xmlns:mml="http://www.w3.org/1998/Math/MathML"><mml:mrow><mml:mrow><mml:mrow><mml:mrow><mml:mrow><mml:mrow><mml:mrow><mml:mrow><mml:mrow><mml:mrow><mml:mrow><mml:mrow><mml:mrow><mml:mrow><mml:mrow><mml:mrow><mml:mrow><mml:mrow><mml:mrow><mml:mrow><mml:mrow><mml:mrow><mml:mrow><mml:mrow><mml:mrow><mml:mrow><mml:mrow><mml:mrow><mml:mrow><mml:mrow><mml:mrow><mml:mrow><mml:mrow><mml:mrow><mml:mrow><mml:mrow><mml:mrow><mml:mrow><mml:mrow><mml:mrow><mml:mrow><mml:mrow><mml:mrow><mml:mrow><mml:mrow><mml:mrow><mml:mrow><mml:mrow><mml:mrow><mml:mrow><mml:mrow><mml:mrow><mml:mrow><mml:mrow><mml:mrow><mml:mrow><mml:mrow><mml:mrow><mml:mrow><mml:mrow><mml:mrow><mml:mrow><mml:mrow><mml:mrow><mml:mrow><mml:mrow><mml:mrow><mml:mrow><mml:mrow><mml:mrow><mml:mrow><mml:mrow><mml:mrow><mml:mrow><mml:mrow><mml:mrow><mml:mrow><mml:mrow><mml:mrow><mml:mrow><mml:mrow><mml:mrow><mml:mrow><mml:mrow><mml:mrow><mml:mrow><mml:mrow><mml:mrow><mml:mrow><mml:mrow><mml:mrow><mml:mrow><mml:mrow><mml:mrow><mml:mrow><mml:mrow><mml:mrow><mml:mrow><mml:mrow><mml:mrow><mml:mrow><mml:mrow><mml:mrow><mml:mrow><mml:mrow><mml:mrow><mml:mrow><mml:mrow><mml:mrow><mml:mrow><mml:mrow><mml:mrow><mml:mrow><mml:mrow><mml:mrow><mml:mrow><mml:mrow><mml:mrow><mml:mrow><mml:mrow><mml:mrow><mml:mrow><mml:mrow><mml:mrow><mml:mrow><mml:mrow><mml:mrow><mml:mrow><mml:mrow><mml:mrow><mml:mrow><mml:mrow><mml:mrow><mml:mrow><mml:mrow><mml:mrow><mml:mrow><mml:mrow><mml:mrow><mml:mrow><mml:mrow><mml:mrow><mml:mrow><mml:mrow><mml:mrow><mml:mrow><mml:mrow><mml:mrow><mml:mrow><mml:mrow><mml:mrow><mml:mrow><mml:mrow><mml:mrow><mml:mrow><mml:mrow><mml:mrow><mml:mrow><mml:mrow><mml:mrow><mml:mrow><mml:mrow><mml:mrow><mml:mrow><mml:mrow><mml:mrow><mml:mrow><mml:mrow><mml:mrow><mml:mrow><mml:mrow><mml:mrow><mml:mrow><mml:mrow><mml:mrow><mml:mrow><mml:mrow><mml:mrow><mml:mrow><mml:mrow><mml:mrow><mml:mrow><mml:mrow><mml:mrow><mml:mrow><mml:mrow><mml:mrow><</mml:mrow></mml:mrow></mml:mrow></mml:mrow></mml:mrow></mml:mrow></mml:mrow></mml:mrow></mml:mrow></mml:mrow></mml:mrow></mml:mrow></mml:mrow></mml:mrow></mml:mrow></mml:mrow></mml:mrow></mml:mrow></mml:mrow></mml:mrow></mml:mrow></mml:mrow></mml:mrow></mml:mrow></mml:mrow></mml:mrow></mml:mrow></mml:mrow></mml:mrow></mml:mrow></mml:mrow></mml:mrow></mml:mrow></mml:mrow></mml:mrow></mml:mrow></mml:mrow></mml:mrow></mml:mrow></mml:mrow></mml:mrow></mml:mrow></mml:mrow></mml:mrow></mml:mrow></mml:mrow></mml:mrow></mml:mrow></mml:mrow></mml:mrow></mml:mrow></mml:mrow></mml:mrow></mml:mrow></mml:mrow></mml:mrow></mml:mrow></mml:mrow></mml:mrow></mml:mrow></mml:mrow></mml:mrow></mml:mrow></mml:mrow></mml:mrow></mml:mrow></mml:mrow></mml:mrow></mml:mrow></mml:mrow></mml:mrow></mml:mrow></mml:mrow></mml:mrow></mml:mrow></mml:mrow></mml:mrow></mml:mrow></mml:mrow></mml:mrow></mml:mrow></mml:mrow></mml:mrow></mml:mrow></mml:mrow></mml:mrow></mml:mrow></mml:mrow></mml:mrow></mml:mrow></mml:mrow></mml:mrow></mml:mrow></mml:mrow></mml:mrow></mml:mrow></mml:mrow></mml:mrow></mml:mrow></mml:mrow></mml:mrow></mml:mrow></mml:mrow></mml:mrow></mml:mrow></mml:mrow></mml:mrow></mml:mrow></mml:mrow></mml:mrow></mml:mrow></mml:mrow></mml:mrow></mml:mrow></mml:mrow></mml:mrow></mml:mrow></mml:mrow></mml:mrow></mml:mrow></mml:mrow></mml:mrow></mml:mrow></mml:mrow></mml:mrow></mml:mrow></mml:mrow></mml:mrow></mml:mrow></mml:mrow></mml:mrow></mml:mrow></mml:mrow></mml:mrow></mml:mrow></mml:mrow></mml:mrow></mml:mrow></mml:mrow></mml:mrow></mml:mrow></mml:mrow></mml:mrow></mml:mrow></mml:mrow></mml:mrow></mml:mrow></mml:mrow></mml:mrow></mml:mrow></mml:mrow></mml:mrow></mml:mrow></mml:mrow></mml:mrow></mml:mrow></mml:mrow></mml:mrow></mml:mrow></mml:mrow></mml:mrow></mml:mrow></mml:mrow></mml:mrow></mml:mrow></mml:mrow></mml:mrow></mml:mrow></mml:mrow></mml:mrow></mml:mrow></mml:mrow></mml:mrow></mml:mrow></mml:mrow></mml:mrow></mml:mrow></mml:mrow></mml:mrow></mml:mrow></mml:mrow></mml:mrow></mml:mrow></mml:mrow></mml:mrow></mml:mrow></mml:mrow></mml:math>	1> 3 €/mml:	:mn>
385	Platinum-Monolayer Shell on AuNi _{0.5} Fe Nanoparticle Core Electrocatalyst with High Activity and Stability for the Oxygen Reduction Reaction. Journal of the American Chemical Society, 2010, 132, 14364-14366.	6.6	191
386	On the formation of Na nanoparticles in femtosecond-laser irradiated glasses. Journal of Applied Physics, 2010, 107, 064301.	1.1	5
387	Gram-Scale-Synthesized Pd ₂ Co-Supported Pt Monolayer Electrocatalysts for Oxygen Reduction Reaction. Journal of Physical Chemistry C, 2010, 114, 8950-8957.	1.5	54
388	Influence of Epitaxial Growth Orientation on Residual Strain and Dielectric Properties of (Ba _{0.3} Sr _{0.7})TiO ₃ Films Grown on In-Plane Compressive Substrates. Ferroelectrics, 2010, 405, 262-267.	0.3	7
389	Valence electron energy-loss spectroscopy of nanoporous MgO. Applied Physics Letters, 2009, 94, 253105.	1.5	6
390	Tri- and quadri-metallic ultrathin nanowires synthesized by one-step phase-transfer approach. Nanotechnology, 2009, 20, 495605.	1.3	7
391	Structure and Activity of Novel Pt Core-Shell Catalysts for the Oxygen Reduction Reaction. ECS Transactions, 2009, 25, 1023-1036.	0.3	16
392	Microstructures induced by femtosecond laser pulses inside glasses. Journal of Materials Research, 2009, 24, 1983-1988.	1.2	4
393	Highâ€Performance Airâ€Processed Polymer–Fullerene Bulk Heterojunction Solar Cells. Advanced Functional Materials, 2009, 19, 3552-3559.	7.8	80
394	Volume plasmon of bismuth nanoparticles. Solid State Communications, 2009, 149, 111-114.	0.9	13
395	Performance and image analysis of the aberration-corrected Hitachi HD-2700C STEM. Journal of Electron Microscopy, 2009, 58, 111-122.	0.9	49
396	Electrochemical performance of graphene nanosheets and ceramic composites as anodes for lithium batteries. Journal of Materials Chemistry, 2009, 19, 9063.	6.7	109

#	Article	IF	CITATIONS
397	Comparison of Mg L23 edges in MgO and Mg(OH)2—Importance of medium-range structure. Ultramicroscopy, 2008, 109, 122-128.	0.8	7
398	Electron energy loss spectroscopy of Na in Na, Na ₂ O, and silicate glasses. Journal of Materials Research, 2008, 23, 2467-2471.	1.2	12
399	On the dehydration mechanism of Mg(OH)2 by a high-energy electron beam. Journal of Applied Physics, 2008, 104, .	1.1	19
400	The Impact of chemical ordering on the dielectric properties of lead scandium tantalate Pb(Sc1â^•2Ta1â^•2)O3 thin films. Journal of Applied Physics, 2007, 102, .	1.1	21
401	Determination of Ti coordination from pre-edge peaks in Ti <mml:math xmlns:mml="http://www.w3.org/1998/Math/MathML" display="inline"><mml:mi>K</mml:mi>-edge XANES. Physical Review B, 2007, 76, .</mml:math 	1.1	79
402	Annealing effect on dislocations in SrTiO3â^LaAlO3 heterostructures. Journal of Applied Physics, 2007, 101, 064102.	1.1	14
403	Oxygen Bonding in Bismuth Layered Compounds SrBi2Ta2O9. Materials Research Society Symposia Proceedings, 2007, 997, 1.	0.1	0
404	Processing and properties of ferroelectric relaxor lead scandium tantalate Pb(Sc1/2Ta1/2)O3 thin films. Journal of Materials Research, 2007, 22, 217-232.	1.2	13
405	Sodium reconstruction on surface of silicate glasses in transmission electron microscope. Applied Physics Letters, 2007, 91, .	1.5	8
406	Growth process approaches for improved properties of tunable ferroelectric thin films. Journal of the European Ceramic Society, 2007, 27, 3753-3758.	2.8	5
407	In-plane versus out-of-plane dielectric response in the thin-film relaxorPb(Sc1â^•2Ta1â^•2)O3. Physical Review B, 2006, 73, .	1.1	10
408	A NEW MICROSCOPIC MECHANISM FOR FATIGUE BEHAVIOR IN BISMUTH LAYER STRUCTURE FERROELECTRICS. Integrated Ferroelectrics, 2006, 79, 273-280.	0.3	0
409	Ferroelectric properties of polycrystalline bismuth titanate films by Nd3+/W6+ cosubstitution. Journal of Applied Physics, 2005, 97, 084102.	1.1	20
410	B-site doping effect on ferroelectric property of bismuth titanate ceramic. Journal of Applied Physics, 2005, 98, 114104.	1.1	35
411	Structural and dielectric properties of strain-controlled epitaxial SrTiO3 thin films by two-step growth technique. Journal of Applied Physics, 2005, 98, 054105.	1.1	24
412	Strain Relaxation and Dislocation Confinement in Epitaxial SrTiO3 by Two-Step Growth Technique and the Resulting Dielectric Response. Materials Research Society Symposia Proceedings, 2005, 902, 1.	0.1	0
413	Morphology and mobility of 90° domains in La-substituted bismuth titanate. Journal of Physics Condensed Matter, 2004, 16, 4549-4556.	0.7	15
414	Comment on "Model of phase transition induced antiphase boundaries in perovskite and layered perovskite oxides―[J. Appl. Phys.92, 5425 (2002)]. Journal of Applied Physics, 2004, 95, 770-771.	1.1	3

#	Article	IF	CITATIONS
415	Structural and Ferroelectric Properties of Bi4â^'xYxTi3O12 Films. Integrated Ferroelectrics, 2004, 65, 105-115.	0.3	0
416	Mechanical and dielectric relaxation in neodymium-modified bismuth titanate ceramics. Solid State Communications, 2004, 131, 189-193.	0.9	22
417	Internal Friction Study of Neodymium-Modified Bismuth Titanate Ceramic. Integrated Ferroelectrics, 2004, 65, 213-223.	0.3	0
418	Doping effect on the dielectric property in bismuth titanate. Journal of Applied Physics, 2004, 95, 3126-3130.	1.1	185
419	Different domain structures and their effects on fatigue behavior in Bi3TiTaO9 and SrBi2Ta2O9 ceramics. Journal of Applied Physics, 2003, 93, 4784-4787.	1.1	34
420	Transmission electron microscopy study on domain structures in Bi3TiNbO9 ceramics. Microelectronic Engineering, 2003, 66, 825-829.	1.1	13
421	Internal friction study on low-temperature phase transitions in lead zirconate titanate ferroelectric ceramics. Applied Physics Letters, 2003, 82, 109-111.	1.5	16
422	La-doped effect on the ferroelectric properties of Bi4Ti3O12–SrBi4Ti4O15 thin film fabricated by pulsed laser deposition. Journal of Applied Physics, 2002, 92, 5420-5424.	1.1	29
423	Microstructure study of Bi/sub 4/Ti/sub 3/O/sub 12/-SrBi/sub 4/O/sub 15/ and Bi/sub 3.25/La/sub 0.75/Ti/sub 3/O/sub 12/-SrBi/sub 4/Ti/sub 4/O/sub 15/ ceramics. , 0, , .		0
424	Stacking Fault Formation via 2D Nucleation in PVT Grown 4H-SiC. Materials Science Forum, 0, 821-823, 85-89.	0.3	2